Predicting the yield strength of a 3D printed porous material from its internal geometry

Martin Lesueur[a,*], Thomas Poulet[b], Manolis Veveakis[a]

[a] *Civil and Environmental Engineering, Duke University, Durham, USA*
[b] *CSIRO Mineral Resources, Perth, Australia*

Abstract

The design of any manufactured material requires the knowledge of its limit of elasticity, called yield strength. Whilst laboratory experiments are currently necessary to do so, this study is part of initiatives which aim at deriving the yield with simple and fast numerical simulations. The seminal work of Gurson (1977) on a simplified pore structure, a single spherical pore, first provided a theoretical relationship between the yield and the porosity, showing that the presence of pore space is responsible for lowering the yield strength. The complexity of new structures requires however to take explicitly into account the internal geometry, usually using direct numerical simulations. This can be particularly complex since the yield strength of a structure is actually reached after some of its parts have already entered the plastic regime. Therefore, the mere computation of the structure's yield strength currently necessitates the modelling of the full plastic behaviour of the skeleton's material. This contribution proposes to simplify the numerical modelling needed for the sole computation of the porous material's yield strength, by postulating that the yielding of a porous material is mostly controlled by the geometry of its internal structure. We show that the influence of that internal geometry on the yield could be retrieved from a finite element computation with just an ideal elasto-plastic material equivalent of the skeleton's. We showcase the predictive power of the method against an

*Corresponding author
Email address: martin.lesueur@duke.edu (Martin Lesueur)

experimental testing, initially benchmarked for 3D-printed samples with either a unique spherical void or a grid infill, before demonstrating its applicability on a complex 3D-printed rock microstructure, reconstructed from segmented micro-Computerised Tomography scans.

Keywords: Yield strength ; Internal geometry ; 3D printing

1. Introduction

The influence of a structure's internal geometry on its mechanical properties is a subject of numerous studies, whether on elastic modulus [30, 17], yield strength [11, 18, 15, 14], or plastic flow law [15, 14]. This contribution focuses on strength, which is necessary for the design of structures to prevent them from entering the plastic regime and suffer irreversible deformations. In that regard, research is striving to design lightweight materials that keep a high strength for the aforementioned purpose. While searching for improved material properties is a possible path, optimisation of the internal geometry of the material is the other one, of interest to this study. This objective is particularly adapted to 3D printed parts [7, 28, 6, 4, 13, 34]. Indeed, 3D printing allows a complete control of the internal geometry of the part and new types of internal geometries that would otherwise be hard to produce can now be envisaged (see the particular example of Build-to-last [28]).

The only unambiguous determination of mechanical yield point, as a limit of elasticity, is restricted to the simplest case of ideal non-porous linear elastic and ideally plastic materials, like metals for instance. Indeed, experimental compression tests of such materials lead to characteristic stress-strain curves displaying a sharp transition between the linear elasticity and plasticity, where strain increases at constant stress. For more complex materials, however, including viscoplastic materials like 3D printed plastics or real geomaterials like porous rocks, the notion of macroscopic yield stress is more ambiguous and its determination dependent on the method selected. To alleviate this ambiguity we use the following three definitions of yield from the sixth edition of the

McGraw-Hill Dictionary of Scientific and Technical Terms [31]:

- ***yield*** *[MECHANICS] That stress in a material at which plastic deformation occurs.*
- ***yield point*** *[MECHANICS] The lowest stress at which strain increases without increase in stress.*
- ***yield strength*** *[MECHANICS] The stress at which a material exhibits a specified deviation from proportionality of stress and strain.*

The first definition, referred to as **initial yield** in this contribution corresponds to the stress when the first region in the material undergoes plasticity. This value is not particularly useful since not easily measurable [8]. The second definition, commonly named **limit load**, points to the state of collapse of the material. The last definition is the **macroscopic yield**, which points to the limit of linear elasticity at the scale of the sample, necessary to design structures. Since the initial yield is particularly impractical to measure and the limit load does not exist in many cases, we focus in this study on the macroscopic yield. Additionally, it is a necessary parameter for any modelling of plasticity. This yield strength is typically measured experimentally on stress-strain curves using the classical offset method [35], as the intersection of the curve with a line parallel to the initial linear-elastic part of that curve, shifted by an ad-hoc strain threshold. In this contribution, following Lesueur *et al.* [24], the macroscopic yield is measured on stress-strain curves with an energetic method, which provides similar values but with stronger physical meaning. Currently, the influence on strength of default types of infill patterns and a few more complex geometries have already been measured [see 36, and references therein]. However, with the rise of complex and unique internal geometries designed for strength-to-weight optimisation, it is necessary to find a simpler and faster way to measure the yield than laboratory experiments.

The first possibility is to assess the yield as a function of porosity [16, 15, 14], the simplest parameter characterising the internal geometry. Through these models, we know that the presence of pore space is responsible for lowering the yield strength value. While that type of analysis was an important first step in our understanding of the influence of the internal geometry, its applicability is restricted to the limit load value due to the use of limit analysis for the modelling. Corresponding results have not yet been derived for the more practical definition of yield, the macroscopic yield. In addition, porosity, as a scalar field, only represents one of the characteristics of the internal geometry [3] and can therefore not capture all geometrical effects, with more work remaining from a more general perspective. In the case of 3D printed parts, it is directly the internal geometry of the unit cell, also referred as infill pattern. In the case of natural materials, bones or rocks for example, it is delimited in segmented micro-Computerised Tomography (µCT) scans by the pore space boundary, also referred as microstructure.

The only other alternative is to perform direct numerical simulation in order to compute the stress-strain curve of the structure, from which to derive the yield. With recent computational advances, it is now possible to simulate mechanical deformation of a Representative Element Volume (REV) of the porous material (e.g. [27]). At that size, the mechanical behaviour of the volume considered should be representative of the whole structure at the larger scale. Therefore stress-strain curves of the REV can be produced numerically that are comparable to the experimental ones. However, reproducing numerical stress-strain curves of real materials remains difficult. An important source of computational cost comes from the fact that non-trivial constitutive plastic law are usually implemented to reproduce the behaviour of the material. Indeed, characterising the plastic behaviour of a real material is no easy feat as there exist numerous constitutive models [29], some of which that require many parameters to be calibrated [26]. Additionally for geomaterials, that cost is then amplified by the size of the mesh, noting that high resolutions are needed to match the REV with accurate grain shapes.

The main complexity of deriving the yield numerically comes from the fact that the full plastic behaviour of the material seems to be needed even to obtain only the structure's yield strength. In this contribution, we propose to simplify the numerical modelling needed for the sole computation of the structure's yield strength, without perceptible loss of accuracy on the result. By narrowing our study to the determination of yield, we only need to simulate the initial phase of plasticity. The plastic regime starts at the initial yield since theoretically speaking, the structure is, from that point on, undergoing localised plastic deformations. However, for porous materials, it is instinctive that the initial yield does not coincide with the macroscopic yield. Localised heterogeneities of the internal geometry will indeed fail before the overall response of the structure can visually deviate from linearity [8]. Under ongoing deformation, from the initial yield to the macroscopic yield, an arbitrarily small plastic strain is accumulated (as defined by the offset method). However, we conjecture that plasticity does not noticeably affect the structure's response until the macroscopic yield. This hypothesis is tested in this contribution by verifying that the yield of a porous material is equal to the one of a virtual porous material with an equivalent ideal elasto-plastic skeleton, instead of considering its more realistic plastic behaviour (including rheology).

To validate the approach proposed, we first select two simple structures allowing their internal geometry to be very accurate, therefore improving reproducibility of this benchmark. The second part of this contribution presents an application for a more complex internal geometry, reconstructed from a rock's segmented µCT scans.

2. Material and methods

The material selected in this contribution is 3D printed polylactic acid (PLA), whose mechanical response from laboratory experiments is plotted in Fig. 1 and modelled in this section, in order to calibrate the skeleton material for the simulations of the following sections. 3D printing presents great advantages for the experimental validation of our approach. As observed by the superposition of curves in Fig. 1 or A.8, the printed samples have a very repro-

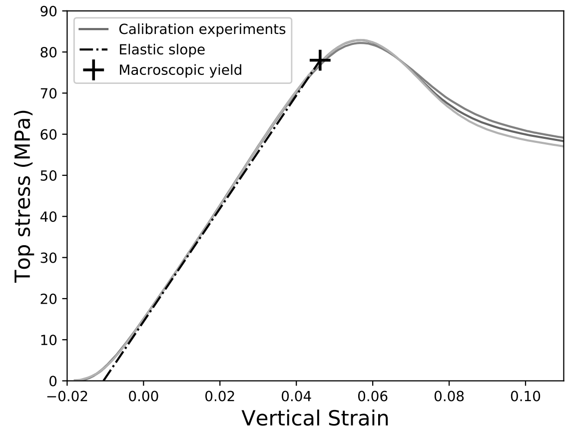

Figure 1: Three stress-strain curves of uniaxial compression of 3D printed identical full cylinders of PLA to observe the plastic response of the material and assess the reproducibility of mechanical tests on 3D printed samples. Our suggested elasto-plastic model is superposed to the curves and determined by two parameters: the slope of the linear elastic region and the macroscopic yield value.

ducible behaviour, to a precision level hard to obtain experimentally on natural materials. In addition, the 3D printing technique allows a perfect control of the internal geometry of the samples, whose influence we are characterising. 3D printed PLA is also particularly well-suited to test our hypothesis because its plastic response is far from ideal plastic. Its complex behaviour, such as its viscoplasticity, has been extensively characterised [10, 22]. The samples display in this contribution both hardening and then softening, as shown in Fig. 1. Moreover, the printing process itself influences the plastic properties of the resulting part, as discussed in this section, which adds an extra layer of complexity. It is therefore extremely interesting to select this material to test our approach, which eliminates the need for characterising the viscoplasticity of the printed PLA.

2.1. 3D printing and mechanical testing procedure

In recent years, many 3D printing methods have been made available, see review from Dizon *et al.* [10]. Without loss of generality we choose to work with the standard Fused Deposition Modeling (FDM) on the Ultimaker 3 machines of the Innovation co-Lab of Duke University, with a nozzle of 0.4 mm diameter. The machine offers the possibility to print multiple materials (see exhaustive list[1] from the manufacturer), with polylactic acid (PLA) and acrylonitrile butadiene styrene (ABS) two of the most commonly used in mechanical testing of 3D printed parts [33, 10]. Without any preferences, we choose to work with PLA.

Many of the printing settings influence the mechanical properties of the printed part, as can be seen in the extensive review of Popescu *et al.* [33] as well as Appendix A and the references therein pointing to studies on the influence of slicing parameters, building orientation and temperature conditions. It is therefore important to keep those parameters constant for consistency purposes between all samples preparation. Starting from the default settings of the 3D printer, we keep the infill density at 100% in order to have a non-porous sample. For the building orientation, the parts are printed vertically and each layer is printed with a rotation of 90 degrees from the previous one in order to reduce the anisotropy of the printing that you would obtain when stacking directly the filaments on top of each other. For the temperature conditions, we follow the recommendation of the Ultimaker 3 user manual for PLA[2] for the extruder's temperature at 200ºC and the one of the bed table at 60ºC. For the slicing parameters, the wall/shell thickness of the part is taken to be equal to the layer height in order to be printed with a single filament in size. Finally, the printing speed is set to 30 mm/s which produces a part of good quality.

All the compression tests presented in this contribution were performed on the HM3000.3F load frame, manufactured by Humboldt Mfg. Co., with a max-

[1] `http://ultimaker.com/materials`

[2] `http://ultimaker.com/en/resources/22225-how-to-print-with-ultimaker-pla`

imum loading capacity of 50 kN. In order to measure the stress on top of the sample, we use the HM-2300.100 S-Type load cell, which has the same load capacity as the machine and is also manufactured by Humboldt Mfg. Co. The strain is measured directly from the speed of the load plate and it was verified that the deformation of the load cell, which is taken in account with this method, had a negligible effect on the results. As a polymer, PLA naturally remains viscoplastic after the printing process and the actual value of the experimental loading rate should therefore influence the results. However, since this contribution is not focused on quantifying the rate-dependency of the mechanical response, we select an arbitrary loading rate of 0.08 mm/min for all experiments in this contribution.

2.2. Mechanical model for 3D printed PLA

In this subsection we propose an elasto-plastic model for PLA, 3D printed as described above, to fit the stress-strain curves of Fig. 1.

The experimental results show that the material does not behave in a linear elastic manner at first but rather displays a non-linear phase due to strain measurement errors [23] (e.g. bedding error). Relatively quickly, however, the material follows a linear elastic response once the top stress value reaches a threshold of approximately 5 MPa. In order to remove the inconsistent bedding error, we shift the origin of vertical strain of each stress-strain curve so it corresponds to the stress value of 15 MPa, a safe arbitrary value above which linear elasticity is fully observed.

The superposition of the elastic part of all curves indicate that the elastic properties are extremely consistent between all samples. We can then measure a Young's modulus of 1375 MPa from the slope of the elastic part in uniaxial compression. Since Poisson's ratio does not play a role in uniaxial compression, we assume the value reported in the literature of 0.45 for our numerical model, as the material is known to be quite incompressible.

The hypothesis tested in this contribution is that we do not need to model the full plastic behaviour of the skeleton material, which, for 3D printed PLA,

Table 1: Mechanical properties measured on uniaxial compression of full samples, for the calibration of simulations. Calibration on the cylinders, plotted on Fig. 1, corresponds to the simulation of Fig. 3 ; The cuboids to the simulation of Fig. 4 ; The cubes to the simulation of Fig. 6.

Sample shape	cylinder	cuboid	cube
Height (mm)	33	21	22
Loading area (mm^2)	$\pi\times 11^2$	21×18.26	22×22
Young's modulus (MPa)	1375	956	875
Macroscopic yield (MPa)	78.0	62.5	70.0

corresponds to a phase of hardening first, due to viscoplasticity, then softening, due to shearbanding. We choose instead to simplify the constitutive plastic modelling to the minimum and idealise the material by considering a J2 rate-independent plasticity model with no hardening or softening. This model needs only one parameter, the value of macroscopic yield. It is measured with the energetic method of Lesueur *et al.* [24], at 78 MPa, displayed as a cross on Fig. 1.

Note that the model selected here is only presented for the specific printing settings and with the testing procedure detailed in the previous subsection and may not be applicable with other parameters as we have shown – non-exhaustively – that many parameters influence the mechanical properties of the printed PLA. For the sake of accurate benchmarking in this contribution, calibration of the Young's modulus and macroscopic yield were made for every different external shapes considered, summarised in Table. 1.

3. Results

3.1. Prediction of the internal geometry's influence on 3D printed PLA yield

The objective of this subsection is to verify if a simplified numerical model can correctly predict the yielding of printed PLA samples with given internal geometries. We select two type of structures. The first one is the simplest internal geometry one can think of, a unique spherical pore. Despite its simplicity, this type of geometry is used as infill pattern [12], and spherical-like voids are particularly suited for complex infill patterns computed by optimisation algorithms [7, 28, 4, 34]. The second geometry tested represents an example of a more classical infill pattern: the grid structure.

The spherical void is enclosed in a cylinder. Two samples are printed, of varying diameter of the spherical void, specifically of 0.6 and 0.7 (normalised to the cylinder diameter). Due to the FDM principle of printing, the molten filament is deposited vertically on the sample, which makes it impossible for this technique to print perfectly any overhanging part with an angle greater than 45º. Unfortunately, this is the case of the spherical void with the overhang going to 90º at the top of the sphere. To help the printing, FDM usually relies on printing under these overhangs some support structure that the user can remove after the print is finished. However, our overhang is fully enclosed in the part so this technique cannot be used. Still, by assessing the quality of the print visually by cutting the sample after the experiments, as shown in Fig. 2a, we can see that the quality of the print remained acceptable, even though imperfect. Indeed, during the mechanical compression, this top part of the sphere is the location which experiences the minimum of stress overall. The grid infill is printed in a cubic sample and the pattern remains the same in one direction, corresponding to an extrusion in this direction. In order not to have the overhang problem discussed above, the sample was printed in the direction of the infill (shown in the direction of the camera in Fig. 2b), perpendicular to the direction of loading (corresponding to vertical in Fig. 2b).

The samples are subjected to uniaxial compression and the experimental results are plotted in Fig. 3 for the two different sphere diameters and in Fig. 4 for the grid infill. Note that each test is repeated two times for reliability reasons. The good superposition of all curves shows that the results of hollow samples experiments are as reproducible as the full ones. The resulting curves for the porous cylinders and cubes display sequentially a hardening and a softening phase. All in all, the mechanical behaviour of the porous samples are very similar to the one for a full sample but with increasingly lower and faster transition to

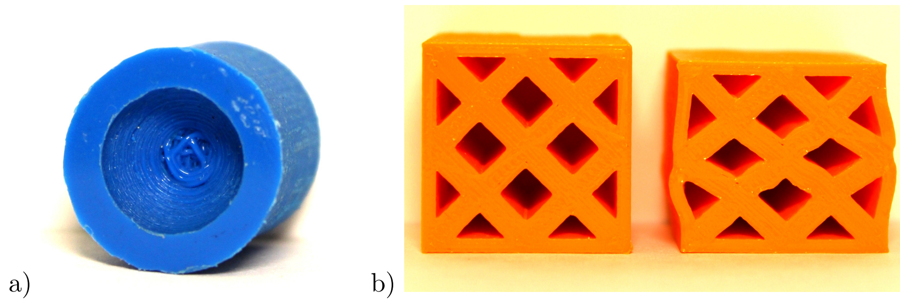

Figure 2: Visualisation of the printed samples of Sec. 3.1. a) is a top-view of the spherical void of the hollow cylinder. Only the top half of the hollow cylinder was printed for visualisation purposes. b) shows the printed cube with grid infill pattern both undeformed (left) and past the yield point (right).

plasticity as porosity increases.

In this section, we are looking at predicting the influence of the internal geometry on the macroscopic yield point of the printed PLA samples. We use the mechanical simulator of the Finite Element platform MOOSE [32] for all numerical simulations in this contribution. It solves for the momentum balance of the skeleton of the porous material. In our simulation, the skeleton's material is attributed the elastic parameters measured for the printed PLA and for the plasticity, we use a $J2$ rate-independent model with no hardening or softening, defined by a single parameter, the yield point of the material, calibrated from Fig. 1 in Sec. 2.2.

The simulation is performed for each structure considered, using the adequate mesh. The cylinders containing a spherical void were meshed with second order tetrahedra and the cube with a grid infill was meshed with first order prisms, resulting from the extrusion of the 2D infill pattern, meshed with triangles. The results are displayed in Fig. 3 for the spherical voids and in Fig. 4 for the grid infill, following the layout introduced in Fig. 1. The stress value of the macroscopic yield of the porous material is reported as a cross on the elastic slope in dashed, both measured from the stress-strain curve produced by the simulation.

The comparison of the numerical and experimental results of Fig. 3 and 4,

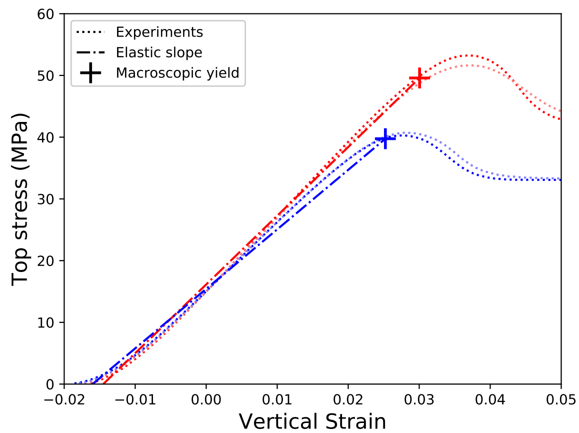

Figure 3: Stress-strain curves of uniaxial compression of 3D printed cylinders of PLA containing a spherical void of different normalised diameters: 0.6 in red and 0.7 in blue. The results of the simulation (elastic slope and macroscopic yield) using the model presented in Sec. 2.2 are superposed to the experimental results.

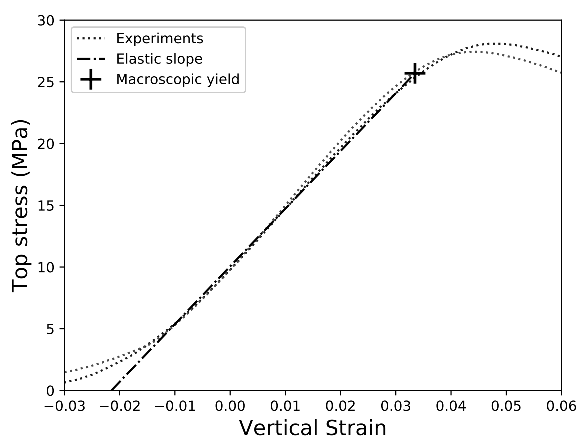

Figure 4: Stress-strain curves of uniaxial compression of 3D printed cuboids of PLA with a grid infill. The results of the simulation (elastic slope and macroscopic yield) using the model presented in Sec. 2.2 are superposed to the experimental results.

Table 2: Mechanical properties measured for the experimental and numerical results of the uniaxial compression of Sec. 3.1.

Internal geometry	spherical void, diameter 0.6			spherical void, diameter 0.7			grid-infill pattern		
Specimen number	exp 1	exp 2	**simulation**	exp 1	exp 2	**simulation**	exp 1	exp 2	**simulation**
Young's modulus (MPa)	1215	1181	1113	1123	1122	964	494.5	527.0	467.5
Macroscopic yield (MPa)	49.30	47.34	49.59	36.88	37.58	39.75	24.0	22.5	25.5

quantified in Table. 2, shows that the simulation is matching closely the macroscopic yield obtained experimentally. Interestingly, this perfect fit demonstrates that the influence of the internal geometry on a structure's yield can be retrieved even with an idealised model of the skeleton's material, without taking into account its real intrinsic behaviour. This verification validates the hypothesis suggested in the introduction that plasticity has little influence on the porous material's behaviour before the macroscopic yield. Particularly, we showed in this section that the hardening and softening behaviour of the 3D printed PLA does not influence the value of the macroscopic yield in these benchmarking examples. This conclusion highlights the potential of the numerical approach to extract the impact of the internal geometry on the structure's yield despite an idealised modelling of the material.

3.2. Application to complex internal geometry

The previous section presented homogenisation results of the macroscopic yield stress for periodic structure with simple unit cells, namely spherical or squared voids. However, natural microstructures of materials usually do not present such perfect unit cells and rely on the concept of REV that needs to be reached in order to obtain accurate homogenised results, representative of a larger scale. As a natural extension of our previous study, we therefore select a rock's microstructure as a more complex geometry in this section for further validation of the suggested approach. The selected rock is a 0.5 mm^3 subsample of the Berea sandstone [20].

Using the stack of segmented 2D µCT scan images, the geometry is meshed

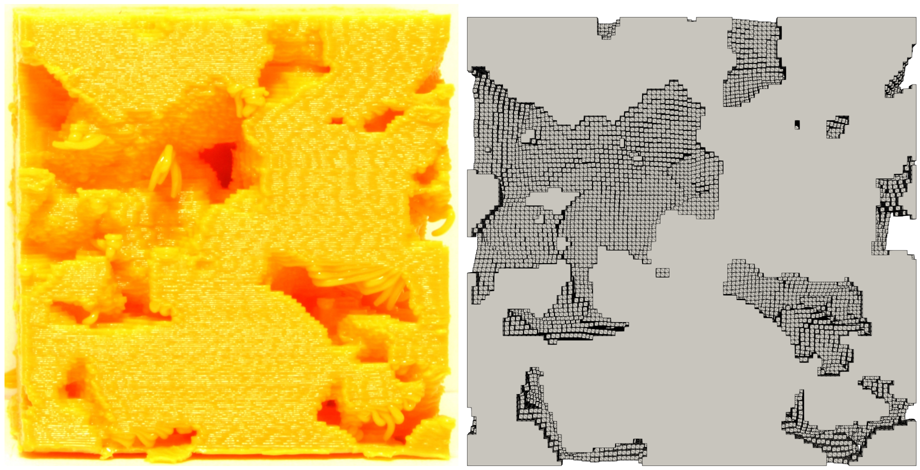

Figure 5: Side face of the printed microstructure (a) compared to the digital rock (b). The 3D printing was done from bottom to top. The full microstructures can be visualised as 3D figures in Supplementary Material (Fig. S1).

in 3D following the methodology described by Lesueur *et al.* [25]. In order to be processed by the Ultimaker 3 machine for printing, the mesh is converted to an STL file format. The sample is printed as a cube of 22 mm^3 size. The quality of the printed sample is quite remarkable in terms of details, capturing very well the overall complexity of the original rock, even though the quality of the print remains imperfect, as can be seen in Fig. 5, due to the 45º limit of any overhang discussed in Sec. 2.1. The printing quality can be assessed by comparing the two 3D figures (see Fig. S1 in Supplementary Material) that visualise the pore space respectively from the original µCT scan and the 3D printed version which was µCT scanned after being printed.

Five identically printed samples are then tested in uniaxial compression following the experimental procedure described in Sec. 2.1. The resulting stress-strain curves, plotted in Fig. 6, all have the same general shape, including the same elastic properties and plastic hardening, but noticeably different values of macroscopic yields. We can only infer that the lack of reproducibility is due to the insufficient printing resolution and quality because the curves of Fig. 3 and 4, whose samples' printing quality was high, superposed completely. Compared to Fig. 3, the complex internal structure plays a different role than the idealised single pore: the sample shows no softening, but instead hardens continuously. The complex pore network in the µCT scan results in a very disperse pore collapse over the whole sample (see plastic deformations in Fig. 7) that could prevent therefore a homogeneous shearband to form, which would explain the absence of softening.

In order to numerically determine the yield of this sample, we simulate the same compression on a digital version of that same microstructure, reconstructed from µCT scans and meshed following the method of Lesueur *et al.* [25], with 796,636 structured elements. The skeleton material implements the ideal elasto-plastic model of 3D printed PLA, described and calibrated in Sec. 2.2.

Despite the fact that the match of Fig. 6 is not as impressive as the one from Fig. 3 and 4, the numerical and experimental curves still match qualitatively and display a similar shape. In this more complex application, the porous material appears to be stiffer and stronger (higher macroscopic yield) with the experimental approach. This could be explained by the reinforcement of the structure due to the existence of artificial bridges between pores that were created during the imperfect printing process. The suboptimal printing quality adds to the uncertainty of the experimental results, which brings us more confidence in the value of elasticity and macroscopic yield determined with the numerical approach.

4. Discussion

In this contribution, we presented an approach to determine the macroscopic yield of a porous material from Finite Element compression of its internal structure, replacing the traditional destructive testing approach. By focusing the study on the macroscopic yield instead of the full mechanical behaviour, we have shown that the complex skeleton material can be satisfactorily approximated by an equivalent ideal elasto-plastic material before reaching the macroscopic yield. By reducing the complexity of the material implemented,

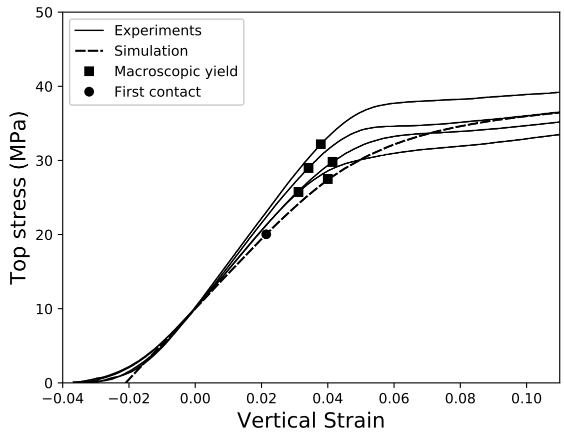

Figure 6: Experimental and numerical stress-strain curves of the uniaxial compression of 3D printed samples of the Berea sandstone [20].

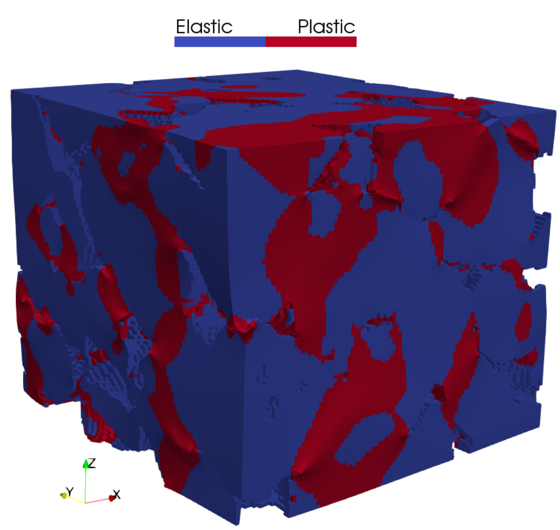

Figure 7: Visualisation of plastic deformations on the numerical uniaxial compression of Fig. 6 at 12% strain.

simulations of mechanical compressions become more accessible.

The new approach was validated on 3D printed PLA. The homogeneity of this material and the reproducibility of the 3D printing techniques makes it a material very suitable for our approach. Furthermore, we show in Sec. 2.2 that the plastic behaviour of the material would present a difficult calibration for modelling purposes, as it depends on many printing parameters. This justifies the use of our approach which disregards this exact plastic behaviour. On the other side, elastic properties and strength of 3D printed materials are being heavily characterised, even though they still require destructive testing to account for their scaling laws with regards to the printing settings. After this calibration step, the rest of the method comes as a convenient non-destructive tool to assess the strength of the numerous customised infill patterns for 3D printed parts being generated by computer algorithms [28, 13, 4, 34]. Furthermore, a universal model for the elasticity and strength of 3D printed materials depending on the printing settings could be expected in the near future [see 5, for the layer height for example], which would alleviate the need for any destructive testing in our methodology.

Successful validation of the approach against simple and complex internal geometries demonstrated the potential for general applicability of the method. In order to refine the benchmarking of complex internal geometries, more suitable 3D printing techniques could be used in order to obtain a quality high enough to obtain perfectly reproducible and therefore trustful results. Indeed, 3D printing µCT scans with high resolution was achieved for instance by Ishutov *et al.* [21].

Since the method was validated against an already challenging material, 3D printed PLA, that displays softening and hardening behaviour, we expect the approach to apply also for a wider range of materials such as geomaterials. To improve the accuracy of our approach in this case, contact mechanics could be implemented as we have shown in Fig. 6 that contacts in a real rock microstructure happen early on the stress-strain curve. It is however unclear if this would affect the macroscopic yield. In any case, contact forces have been known to be responsible for the pressure sensitivity of the yield surface at the macro-scale, modelled commonly with a Drucker-Prager which characterises a wide array of geomaterials.

In summary, this study aimed at highlighting the predictive power scientific community can develop as 3D printing technology is maturing, at a level of quality where reproducible mechanical compression experiments on 3D printed samples can be performed. We showed that the macroscopic yield can be obtained for a given internal geometry from 3D printed reproductions, for high enough resolutions. More importantly, it was shown that it can also be predicted numerically, in a non-destructive manner, using the simplest plasticity model for the actual skeleton material. This result has striking repercussions for a number of applications, including 3D printed scaffolds, or even more for real materials like bones or geomaterials, whose internal structure can be obtained from µCT scans. Given that 3D printing and numerical simulations are approaching their originally anticipated goal of providing invaluable insight to the mechanical properties of natural materials, studies like the present one are aiming at opening the door to an enhanced material design era.

References

[1] 3D Matter, 2015. What is the influence of color, printing speed, extrusion temperature and ageing on my 3d prints? http://my3dmatter.com.

[2] Ahn, S.H., Montero, M., Odell, D., Roundy, S., Wright, P.K., 2002. Anisotropic material properties of fused deposition modeling ABS. Rapid Prototyping Journal 8, 248–257. doi:`https://dx.doi.org/10.1108/13552540210441166`.

[3] Arns, C., 2009. Structure-property Relationships from Digital Images. VDM Verlag. URL: `https://www.ebook.de/de/product/8210630/christoph_arns_structure_property_relationships_from_digital_images.html`.

[4] Belhabib, S., Guessasma, S., 2017. Compression performance of hollow structures: From topology optimisation to design 3d printing. International Journal of Mechanical Sciences 133, 728–739. doi:10.1016/j.ijmecsci.2017.09.033.

[5] Bell, D., Siegmund, T., 2018. 3d-printed polymers exhibit a strength size effect. Additive Manufacturing 21, 658–665. doi:10.1016/j.addma.2018.04.013.

[6] Belter, J.T., Dollar, A.M., 2015. Strengthening of 3d printed fused deposition manufactured parts using the fill compositing technique. PLOS ONE 10, e0122915. doi:10.1371/journal.pone.0122915.

[7] Bickel, B., Bächer, M., Otaduy, M.A., Lee, H.R., Pfister, H., Gross, M., Matusik, W., 2010. Design and fabrication of materials with desired deformation behavior. ACM Transactions on Graphics 29, 1–10. doi:10.1145/1778765.1778800.

[8] Desrues, J., Andò, E., Bésuelle, P., Viggiani, G., Debove, L., Charrier, P., Toni, J.B., 2017. Localisation precursors in geomaterials?, in: Springer Series in Geomechanics and Geoengineering. Springer International Publishing, pp. 3–10. doi:https://dx.doi.org/10.1007/978-3-319-56397-8_1.

[9] Divyathej, M.V., Varun, M., Rajeev, P., 2016. Analysis of mechanical behavior of 3d printed abs parts by experiments. International Journal of Scientific & Engineering Research 7, 116–124. URL: https://www.ijser.org/researchpaper/Analysis-of-mechanical-behavior-of-3D-printed-ABS-parts-by-experiments.pdf.

[10] Dizon, J.R.C., Espera, A.H., Chen, Q., Advincula, R.C., 2018. Mechanical characterization of 3d-printed polymers. Addit. Manuf. 20, 44–67. doi:https://dx.doi.org/10.1016/j.addma.2017.12.002.

[11] Dunn, D.E., LaFountain, L.J., Jackson, R.E., 1973. Porosity dependence and mechanism of brittle fracture in sandstones. J. Geophys. Res. 78, 2403–2417. doi:https://dx.doi.org/10.1029/jb078i014p02403.

[12] Galeta, T., Raos, P., Stojšić, J., Pakši, I., 2016. Influence of structure on mechanical properties of 3d printed objects. Procedia Engineering 149, 100–104. doi:10.1016/j.proeng.2016.06.644.

[13] Gopsill, J.A., Shindler, J., Hicks, B.J., 2017. Using finite element analysis to influence the infill design of fused deposition modelled parts. Progress in Additive Manufacturing 3, 145–163. doi:10.1007/s40964-017-0034-y.

[14] Green, R.J., 1972. A plasticity theory for porous solids. Int. J. Mech. Sci. 14, 215–224. doi:https://dx.doi.org/10.1016/0020-7403(72)90063-x.

[15] Gurson, A.L., 1977. Continuum theory of ductile rupture by void nucleation and growth: Part i—yield criteria and flow rules for porous ductile media. J. Eng. Mater. Technol. 99, 2–15. doi:https://dx.doi.org/10.1115/1.3443401.

[16] Hamiel, Y., Lyakhovsky, V., Agnon, A., 2004. Coupled evolution of damage and porosity in poroelastic media: theory and applications to deformation of porous rocks. Geophys. J. Int. 156, 701–713. doi:https://dx.doi.org/10.1111/j.1365-246x.2004.02172.x.

[17] Hashin, Z., Shtrikman, S., 1963. A variational approach to the theory of the elastic behaviour of multiphase materials. J. Mech. Phys. Solids 11, 127–140. doi:https://dx.doi.org/10.1016/0022-5096(63)90060-7.

[18] Hoshino, K., 1974. Effect of porosity on the strength of the clastic sedimentary rocks, in: Advances in rock mechanics: Proceedings of the 3rd Congress of International Society of Rock Mechanics, Denver, Colorado, September, pp. 511–516.

[19] Huang, L., Dyaur, N., Stewart, R.R., 2015. Elastic properties of 3d-printed physical models: Fluid substitution observations in cracked media, in: SEG

Technical Program Expanded Abstracts 2015, Society of Exploration Geophysicists. doi:https://dx.doi.org/10.1190/segam2015-5915204.1.

[20] Imperial College Consortium On Pore-Scale Modelling, 2014. Berea sandstone. *figshare* http://dx.doi.org/10.6084/m9.figshare.1153794.

[21] Ishutov, S., Hasiuk, F.J., Harding, C., Gray, J.N., 2015. 3d printing sandstone porosity models. Interpretation 3, SX49–SX61. doi:https://dx.doi.org/10.1190/int-2014-0266.1.

[22] Istif, I., Feratoglu, K., Colak, O.U., Acar, A., 2019. Investigation of tensile, viscoelastic, and viscoplastic behavior of polylactic acid manufactured by fused deposition modeling. Journal of Testing and Evaluation 49, 20180964. doi:10.1520/jte20180964.

[23] Jardine, R.J., Symes, M.J., Burland, J.B., 1984. The measurement of soil stiffness in the triaxial apparatus. Géotechnique 34, 323–340. doi:https://dx.doi.org/10.1680/geot.1984.34.3.323.

[24] Lesueur, M., 2020. Influence of multiphysics couplings across scales: from digital rock physics to induced fault reactivation. Ph.D. thesis. UNSW Sydney. School of Minerals and Energy Resources Engineering.

[25] Lesueur, M., Casadiego, M.C., Veveakis, M., Poulet, T., 2017. Modelling fluid-microstructure interaction on elasto-visco-plastic digital rocks. Geomechanics for Energy and the Environment 12, 1–13. doi:https://dx.doi.org/10.1016/j.gete.2017.08.001.

[26] Lin, J., Sari, M., Alevizos, S., Veveakis, M., Poulet, T., 2020. A heuristic model inversion for coupled thermo-hydro-mechanical modelling of triaxial experiments. Computers and Geotechnics 117, 103278. doi:https://dx.doi.org/10.1016/j.compgeo.2019.103278.

[27] Liu, J., Sarout, J., Zhang, M., Dautriat, J., Veveakis, E., Regenauer-Lieb, K., 2017. Computational upscaling of drucker-prager plasticity from micro-

CT images of synthetic porous rock. Geophysical Journal International 212, 151–163. doi:https://dx.doi.org/10.1093/gji/ggx409.

[28] Lu, L., Sharf, A., Zhao, H., Wei, Y., Fan, Q., Chen, X., Savoye, Y., Tu, C., Cohen-Or, D., Chen, B., 2014. Build-to-last: Strength to weight 3d printed objects. ACM Transactions on Graphics 33, 1–10. doi:10.1145/2601097.2601168.

[29] Lubliner, J., 2008. Plasticity Theory. Dover books on engineering, Dover Publications. URL: https://books.google.com/books?id=MkK-BLbHtcAC.

[30] Mackenzie, J.K., 1950. The elastic constants of a solid containing spherical holes. Proceedings of the Physical Society. Section B 63, 2–11. doi:https://dx.doi.org/10.1088/0370-1301/63/1/302.

[31] Parker, S.P., 2003. McGraw-Hill Dictionary of Scientific and Technical Terms. Sixth ed., New York : McGraw-Hill.

[32] Permann, C.J., Gaston, D.R., Andrš, D., Carlsen, R.W., Kong, F., Lindsay, A.D., Miller, J.M., Peterson, J.W., Slaughter, A.E., Stogner, R.H., Martineau, R.C., 2020. MOOSE: Enabling massively parallel multiphysics simulation. SoftwareX 11, 100430. URL: http://www.sciencedirect.com/science/article/pii/S2352711019302973, doi:https://doi.org/10.1016/j.softx.2020.100430.

[33] Popescu, D., Zapciu, A., Amza, C., Baciu, F., Marinescu, R., 2018. FDM process parameters influence over the mechanical properties of polymer specimens: A review. Polym. Test. 69, 157–166. doi:https://dx.doi.org/10.1016/j.polymertesting.2018.05.020.

[34] Qiu, W., Jin, P., Jin, S., Wang, C., Xia, L., Zhu, J., Shi, T., 2020. An evolutionary design approach to shell-infill structures. Additive Manufacturing 34, 101382. doi:10.1016/j.addma.2020.101382.

[35] Ross, C.T.F., 1999. Mechanics of Solids. Woodhead Publishing.

[36] Suteja, T.J., Soesanti, A., 2020. Mechanical properties of 3d printed polylactic acid product for various infill design parameters: A review. Journal of Physics: Conference Series 1569, 042010. doi:10.1088/1742-6596/1569/4/042010.

Acknowledgements

This work was supported by resources provided by the Australian Research Council (ARC Discovery Grant Nos. DP170104550, DP170104557, Linkage Project LP170100233) and the Pawsey Supercomputing Centre with funding from the Australian Government and the Government of Western Australia. M.V. acknowledges support by the DE-NE0008746- DoE, United States project. All 3D printed parts presented in this contribution were made in Duke University's Innovation Co-Lab, program run by Chip Bobbert.

Appendix A. Printing parameters influencing mechanical behaviour

In this appendix, we provide a study on some less common printing parameters that influence the mechanical behaviour of the 3D printed sample. The list is not exhaustive and more parameters can be found in the extensive review of Popescu *et al.* [33].

Appendix A.1. Relaxation time

A parameter suspected to influence compression tests on 3D printed samples is the time elapsed between the impression and compression of the samples. One can indeed wonder, with the heat treatment that the polymer receives during the printing process, if there is a needed relaxation time for a sample to reach a static steady state once the impression is finished. In this regard, a study [1] measured that the peak stress of the material increases with time after printed until it reaches a steady value after 3 days approximately. To verify and

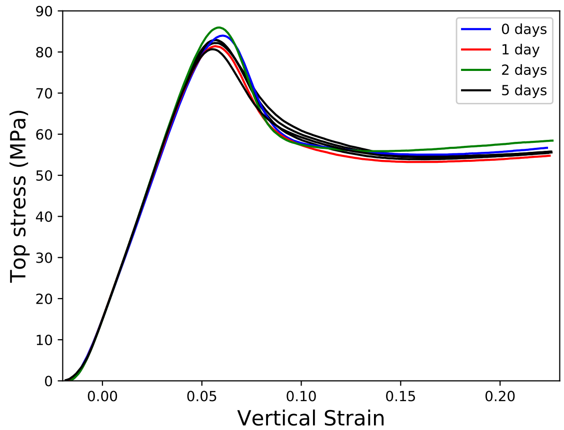

Figure A.8: Stress strain curves of non-porous cylindrical samples of 3D printed PLA for different relaxation times. 0 days means that the sample was tested just after being printed. 4 different curves correspond to 5 days of relaxation.

complete this analysis, we tested this theory on the whole stress-strain response of our samples. The specimens were left next to the machine in the Multiphysics Geomechanics confined laboratory for different periods of time after they are printed. Note that the temperature and relative humidity are monitored to be constant at respectively 22±2°C and 58.8%. Fig. A.8 shows the resulting stress strain curves for different times of relaxation. We observe no difference between the curves and can infer that the relaxation time has no influence on the mechanical behaviour of our samples.

Appendix A.2. Filament size

Another aspect that could influence the results of this study comes from the 3D printing method itself. Compared to injection moulding that creates a sample made of pure homogeneous material, the FDM introduces a notion of internal length scale related to the filament diameter, which is also the layer height in the printer setting. Since the filaments are not fused perfectly, there exist some void gaps between them which results in a global micro-porosity of the printed material. Huang *et al.* [19] measured that this porosity could amount to as much as 4%. This micro-porosity could explain the discrepancy observed between mechanical response of PLA samples printed and moulded [2, 9]. In order to have representative and reproducible results, we need to achieve a good scale separation between the filament size and the sample size, so that the imperfections of printing average out. Another consequence of this internal length scale is that scale separation between the filament size and the sample size was shown to influence the strength of the printed material by Bell *et al.* [5]. We recover the same trend in our study, by observing from the comparison of the cylinder and the cube in Table. 1 that the strength increases with increasing ratio between layer and sample height. And we checked for every structure involved that we are indeed above the printing REV as illustrated by the superposition of the curves in Fig. 3 and A.8.